Simplified fragility-based risk analysis for impulse governed blast loading scenarios

Pierluigi Olmati[a], Francesco Petrini[b], Dimitrios Vamvatsikos[c], Charis Gantes[c]

[a] Tokyo Polytechnic University, Atsugi, Kanagawa, Japan, Email: pierluigi.olmati@gmail.com

[b] Sapienza University of Rome, School of Civil and Industrial Engineering, Rome, Italy,

[c] National Technical University of Athens, School of Civil Engineering, Athens, Greece

Keywords: performance-based design, fragility analysis, safety factor, steel built-up blast resistant door, simplified SDOF model, Monte Carlo simulation.

Abstract

Blast-loaded structures are presently assessed and designed following a deterministic approach, where only a set of structural analyses under worst-case design scenarios are carried out in order to verify each limit state. As a rational alternative, a conditional probabilistic approach is introduced to offer comprehensive risk assessment and to allow the design with user-defined confidence in meeting performance targets in view of uncertainties. To simplify the probabilistic consideration of the uncertain parameters, the determination of the blast hazard and the structural response are decoupled into the evaluation of blast hazard curves and structural fragilities curves, respectively, by introducing a single conditioning intensity measure. This is chosen to be the impulse density, shown to be sufficient for impulse-governed scenarios, achieving a reduction of the computational effort by several orders of magnitude without introducing bias. Furthermore a problem-specific safety factor formulation is introduced to incorporate the influence of uncertainties in a simple manner, akin to current engineering practice. As a proof-of-concept test, a steel built-up blast resistant door is subjected to an accidental detonation of mortar rounds in a military facility. The equivalent single degree of freedom model is adopted in order to conduct the structural analyses, while detailed finite element analyses are carried out for validation. Finally, the conditional approach risk analysis on the steel door is compared against the results obtained through the comprehensive (probabilistic) unconditional approach, showing the validity of both the proposed intensity measure and safety factor formulation.

1 Introduction

As for any structural problem, in order to assess the response of structures subjected to a detonation the following tasks must be achieved:

a) hazard (blast) analysis [1, 2],
b) structural demand assessment (i.e. structural analysis) [2],
c) structure/component capacity assessment [2],
d) safety assessment (i.e., comparison of demand and capacity) [3].

Usually the execution of all of the above steps is conducted in a deterministic rather than a probabilistic way. At the scale of the structural system the global response can be assessed by considering pertinent damage scenarios [4, 5] while at the scale of the single structural element detailed numerical models are employed for the correct prediction of both blast demand [6 - 7] and damage pattern of the structural element [8].

While, generally, the deterministic approach is preferred in order to design structures under blast loads, a number of works can be useful in order to calibrate probabilistic models and bound the uncertainties affecting the design of blast resistant structures. Stewart and Netherton [9] studied two types of window glazing system and investigated the crucial issue of selecting an appropriate intensity measure for computing the fragility curves for blast loaded structures. The fragility curves are developed as a function of two different intensity measures (the explosive weight and the stand-off distance) and several fragility curves are computed for specific cases of study. Netherton and Stewart [10] investigated the accuracy of the blast loading prediction model, concluding that the overall risk is sensitive to uncertainties of the blast load model. An example regarding the complexity of the blast load modeling is shown in the work of Ballantyne et al. [6] where the clearing effect for finite width surfaces is investigated. In the study of Wu et al. [11] a series of different kinds of concrete slabs are tested in order to both compare their blast resistance and evaluate the uncertainty affecting the pressure estimation procedures provided in the Unified Facilities Criteria (UFC) 3-340-02 [2] manual. Chang and Young [12] used Monte Carlo simulations in order to estimate the probability of failure for windows subjected to blast load induced by a vehicle bomb. Low and Hao [13] presented results of a parametric investigation on the reliability of reinforced concrete slabs under blast loading in order to establish appropriate probabilistic distributions of the resistance parameters. Olmati et al. [14] carried out fragility analyses for the performance-based design of cladding wall panels subjected to blast load by adopting the scaled distance as intensity measure, and presented a discussion about the effectiveness of this choice.

The difference between deterministic and probabilistic approach is that in the first case only one blast load scenario is considered in order to define the hazard, usually taken to be representative of the worst case. Then, a single structural model realization, typically incorporating average or characteristic material properties, is analyzed to obtain the corresponding Demand (D) value. Similarly the Capacity (C) is assumed to be a single value describing an upper threshold in the response parameter of interest (e.g. rotation or strain), which when exceeded determines the violation of the limit state. The safety comparison is performed through the well-known equation $C>D$; as a consequence, the result is a binary “safe” or “unsafe” answer.

Conceptually, the probabilistic approach can be considered to be a repetition of the deterministic assessment over many (ideally all) possible scenarios. Then, the safety assessment becomes an evaluation of the probability that the demand exceeds the capacity, formally $P(C<D)$, also known as the probability of exceedance of the limit state that is tied to the capacity. For example, if one considers N_b equally probable blast loadings, N_s equally probable realizations of the structure and N_c equally probable capacity values, then $P(C<D)$ is the fraction of the $N_b \cdot N_s \cdot N_c$ scenarios where the demand exceeds the capacity.

Both the advantages and disadvantages of using the probabilistic approach are well-discussed in the literature [15 - 17]. They mainly revolve around the complexity of applying a probabilistic analysis versus the additional insight, reliability and often economy offered when one takes into account all pertinent uncertainties. The emergence of performance-based engineering and present abundance of computational resources have allowed the adoption of probabilistic methods in many fields of the civil engineering [18 - 23], a trend that is, nowadays, also moving into blast [9, 10, 14, 24]. In view of such advancements, a streamlined method for probabilistic performance-based blast analysis is proposed here for impulse-governed loading of first-mode-dominated structures. Essentially it confers all of its advantages while removing its perceived complexity by having a low computational footprint and closed-form solutions for safety assessment.

2 Probabilistic basis for performance assessment

Assessing the probability of exceedance for any limit state of interest, $P(C<D)$, can be achieved by several procedures that can be broadly categorized in two classes: the unconditional (UA) and conditional (CA) approach. In the unconditional approach, samples of blast scenarios, model

realizations, and potential capacity values are generated, then combined in order to determine P(C<D) by a single Monte Carlo simulation. The unconditional approach is exactly the generation of the $N_b \cdot N_s \cdot N_c$ scenarios described earlier, from which the fraction that violates (exceeds) the limit state is evaluated. The main disadvantage of the unconditional approach is the need for performing $N_b \cdot N_s$ structural analyses, if the value of capacity is assumed not to influence the structural response, or $N_b \cdot N_s \cdot N_c$ otherwise. This has led to the adoption of the so-called conditional approach, widely used in earthquake engineering [25, 26]. Therein, an interface variable, called intensity measure (*IM*), is introduced to be able to fully represent the characteristics of the hazard in a single scalar (or rarely vector) variable. Formally, *IM* needs to be "sufficient" [27]. Then, hazard analysis needs to assess the distribution of *IM* arising from the potential blast scenarios, while structural analysis is reduced to computing the distribution of structural response conditioned on the value of the (scalar) *IM*.

A blast scenario depends on multiple parameters (stand-off distance, charge weight, height of the detonation, presence of barriers, etc.). Conversely, an unconditional approach would involve the determination of structural response over the vector of hazard parameters, leading to a large number of blast scenario realizations N_b and corresponding structural analyses. By introducing a scalar *IM*, the conditional approach effectively reduces the structural analysis effort by several orders of magnitude. Perhaps the only downside is that the probability of exceedance of the limit state is no longer a simple fraction but instead necessitates the integration through the application of the total probability theorem:

$$\mathrm{P}(C < D) = \int_0^{+\infty} \mathrm{P}(C < D \mid IM)\, f(IM)\, \partial IM \qquad (1)$$

The target of structural analysis now becomes the assessment of the conditional probability of exceeding a limit state, P(C<D|IM), the so-called limit state fragility curve or function [28]. P(C<D|IM) is determined for a range of *IM*, ideally from a value of IM=0 to a value that causes the probability of exceedance to become 1, essentially guaranteeing failure. $f(IM)$ is the probability density function (PDF) of encountering a given *IM* value and its determination is the target of the blast hazard assessment. Thus, the problem is efficiently divided in two parts with the benefit that the complete structural characterization, achieved by the fragility curve, can be used for any blast scenario (different charge weights, stand-offs, etc.). As both the demand *D* and the capacity *C* are random variables, the actual evaluation of the probability of exceedance can become more complex than Eq. (1) implies. Following simplifying assumptions and methods from performance-based engineering [29] a useful *IM* for performance-based blast assessment and design will be presented, together with the analytical evaluation of Eq. (1) in a format that is useful for practical applications.

3 The impulse density as intensity measure

Two of the main parameters that determine the blast load on structures are: the scaled distance (Z) and the amount of explosive or charge weight (W). Fig. 1a shows their effect on blast pressure (p) and blast impulse (i) both taken as load parameters for the case of surface burst explosions [2]. The stand-off distance R is measured from the target to the explosive source, while the scaled distance Z is obtained by dividing R by the cube root of the explosive charge weight W. p_0 is the side-on pressure, p_r is the reflected pressure, i_0 and i_r are the side-on and reflected impulse densities, respectively [2]. Based on the UFC 3-340-02 [2] manual the blast load can be defined as an equivalent triangular pulse as indicated in Fig. 1a, where t_d is the equivalent triangular pulse duration. Via the functional relationships shown in Fig. 1a in terms of the scaled distance and explosive weight, a direct dependence of the blast load on both peak pressure p_{peak} (p_r in the case of Fig. 1a) and impulse density (i) can be observed.

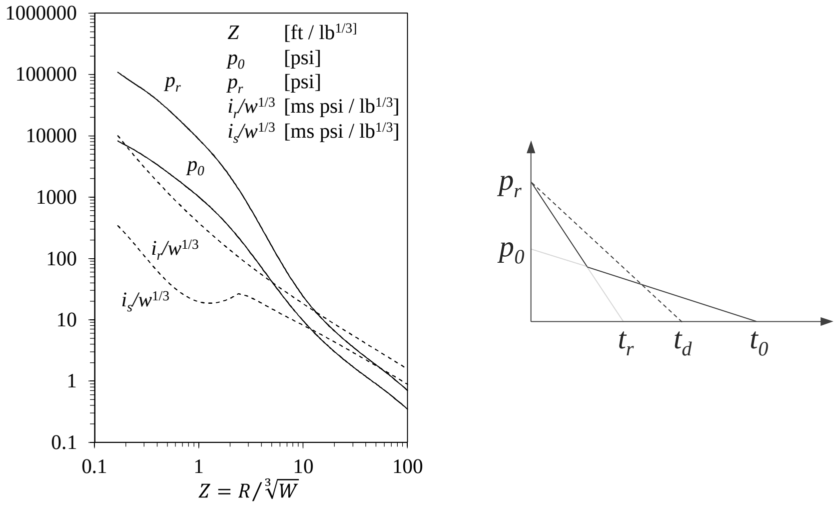

(a) (b)

Fig. 1: (a) Blast load parameters [2]; (b) design blast load shapes [2]

Fig. 2a represents an iso-response curve, i.e., a curve of constant structural demand D (in this case referring to the support rotation θ), plotted as a function of both the peak pressure and the impulse density of the blast load. The chart shown in Fig. 2a is called pressure-impulse diagram and it is very common in blast engineering when designing structural elements [30]. The pressure-impulse diagram indicates that the structural response depends on both peak pressure p and impulse density i. Therefore a comprehensive *IM* to adopt in blast design should be the vector (p,i) and consequently the fragility is best represented by a surface P(D|p,i) instead of a curve P(D|i) or P(D|p). As previously stated, identifying cases where the vector can be reduced to a scalar parameter is advantageous, as it would reduce the computational effort by an order of magnitude.

The relationship between i and p is well known in current design procedures that are based on a single pressure-impulse diagram for a component [31 - 37]. Fig. 2a shows the different regions of the pressure-impulse diagram: i) the impulsive region (I_R) where only the impulse density is relevant for the structural response of a component; ii) the dynamic region (D_R) where the structural response of the component is governed by the load shape and the pressure magnitude; and finally iii) the quasi-static region (S_R) where only the peak pressure is relevant for the structural response of a component. If a probabilistic approach is adopted, an infinite number of such pressure-impulse diagrams should be considered for the specific response level, each one corresponding to a single value of the probability of exceedance between 0 and 1. Each pressure-impulse diagram is a cross section of the above mentioned P(D|p,i) fragility surface, defined by a plane at constant probability of exceedance P_0. Each fragility curve P(D|i), where impulse is the *IM*, is a cross-section of P(D|p,i) defined by a plane at a constant pressure. Fig. 2a shows these cross-sections of the fragility surface that define the fragility curves, each one for a constant value of the pressure. This direct relationship between the constant-pressure fragility curves (Fig. 2a) and the pressure-impulse diagram (Fig. 2a) is crucial because from the fragility curves of Fig. 2a the pressure-impulse diagram for a constant conditional probability of exceedance can be immediately obtained, e.g., as in Fig. 2a. Then, the points of a certain pressure-impulse diagram can be viewed as a series of iso-probability impulse values, each one belonging to a different P(D|i) fragility curve, as shown in the illustrative example of Fig. 2.

The P(D|i) fragility curves of Fig. 2a are practically coincident when the pressure value belongs to the impulsive region. This is because in the impulsive region a change of the pressure does not imply a significant variation of the structural response and, consequently, of the structural fragility. On the other hand, when the pressure value moves toward the dynamic and quasi-static regions the fragility curves become substantially different.

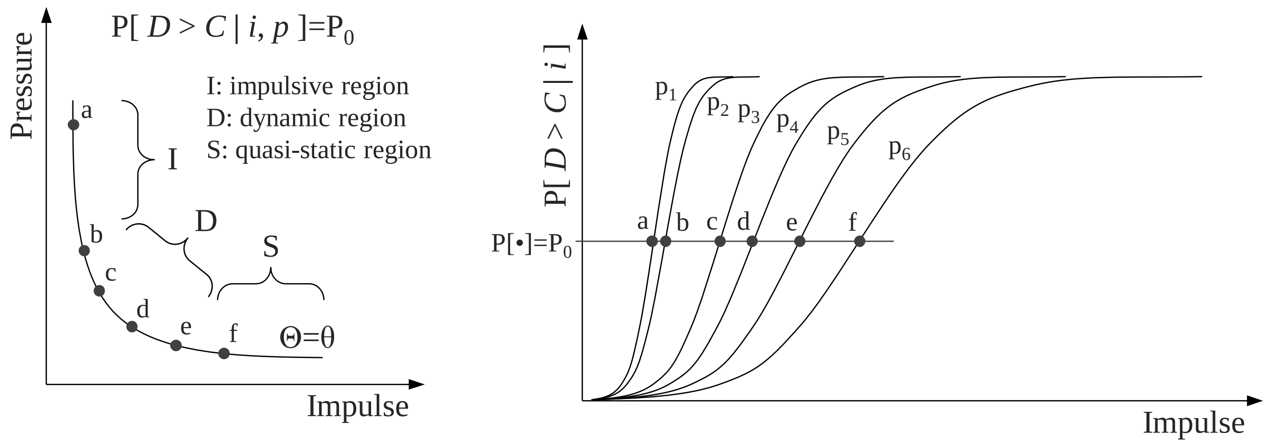

(a) (b)

Fig. 2: Probabilistic description of the blast response for a structural component. (a) Generic pressure-impulse diagram; (b) structural fragility conditioned on impulse for different given pressures p_i (i = 1-6). For p_i in the impulsive region, the curves are essentially coincident.

For most blast-resistant structural elements the loading conditions due to detonations of high potential explosives are generally associated with the impulsive region of the pressure-impulse diagram. Therefore the impulse density (i) is selected as *IM* to characterize the blast load. However, for very stiff and heavy structures, the loading conditions can be on the dynamic or quasi-static region of the pressure-impulse diagram; for this kind of structures the impulse density is an insufficient *IM* and can lead to over estimation of the probability of exceedance (i.e., bias).

In Fig. 3a a general pressure-impulse diagram is shown. The choice of i as intensity measure means that for a pressure value p_0 belonging to the impulsive region of the pressure-impulse curve a range of the impulse Δi can be identified, spanning within points "a" ($P(D>C|i) = \varepsilon$) and "c" ($P(D>C|i) = 1-\varepsilon$) (where ε <<1) in Fig. 3a. In this region, the pressure-impulse curve can be approximated only by its impulsive asymptote. This trend defines a curve representing the structural fragility for impulse sensitive structural elements; see Fig. 3a. In order to obtain the above fragility curve, a number of load samples (pairs of the explosive charge and the stand-off distance) can be considered. Each load sample is defined by both a peak pressure and an impulse density in order to characterize, e.g., the triangular load shape (in the latter case the decay coefficient should also be defined [35]). The load sample should belong to an appropriate region located in the pressure-impulse plane around point "b", as shown in In Fig. 3a.

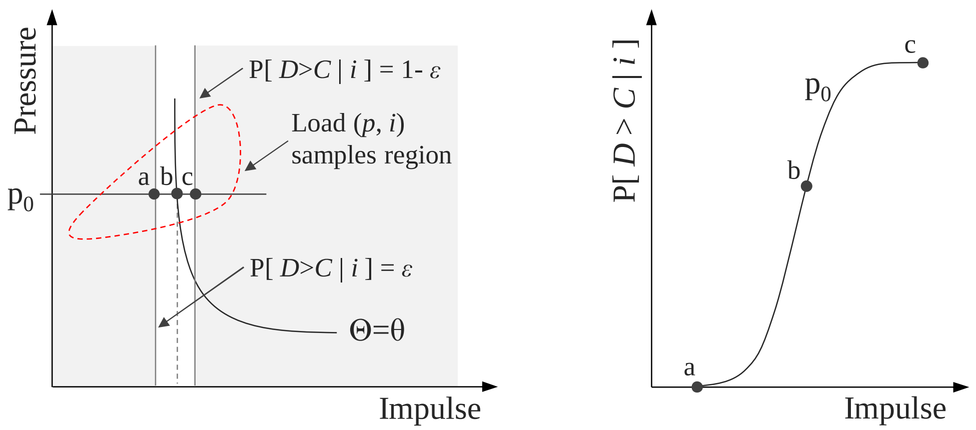

(a) (b)

Fig. 3. Conceptual definition of the fragility curve for impulse sensitive structures

4 Probabilistically-consistent safety factor approach

The evaluation of the integral in Eq. (1) can be simplified by a number of appropriate assumptions. First, both demand *D* and capacity *C* are assumed to be lognormally distributed, having median values of $\hat{\imath}_c$, $\hat{\imath}_D$ and dispersions (standard deviations of the log data) of β_C and β_D. The latter are numerically almost the same as V_c and V_d, the coefficient of variations of the capacity and demand respectively, at least for values less than about 0.6. Then, following the derivation of Cornell et al. [29], it can be shown that for uncorrelated demand and capacity, Eq. (1) becomes:

$$\mathrm{P}(C < D) = 1 - \Phi\left(\frac{\ln \hat{\imath}_C - \ln \hat{\imath}_D}{\sqrt{\beta_C^2 + \beta_D^2}}\right) \qquad (2)$$

Where Φ is the cumulative distribution function (CDF) of the standard normal distribution. If we let *x* represent the Acceptable Probability of Exceedance (APE), Φ^{-1} be the inverse of Φ, and K_{APE} be the standard normal variate corresponding to non-exceedance probability of 1-*x*, then checking for P(*C*<*D*) < *x* can be transformed via Eq. (2) into Eq. (3) and Eq. (4) [29, 38].

$$\lambda = e^{K_{APE}\beta_T} < \frac{\hat{\imath}_C}{\hat{\imath}_D} \qquad (3)$$

where

$$\beta_T = \sqrt{\beta_C^2 + \beta_D^2}\,; \quad K_{APE} = \Phi^{-1}(1 - x) \qquad (4)$$

The safety factor (*λ*) is defined by Eq. (3) and can be broken into familiar demand and capacity factors, each ruled by the corresponding dispersion. Safety checking simply becomes a test of whether the ratio of $\hat{\imath}_c/(\lambda\hat{\imath}_D)$, exceeds 1.0.

The proposed safety factor is thus intended to be applied as multiplier of the median demand intensity for a probabilistically-consistent design of structural elements. Wherever a monotonic relationship is available that connects impulse density (the *IM*) with structural response, this relationship can be used to connect the median response to the median intensity. Then, Eq. (3) can be used to incorporate the effect of uncertainty into design decisions. For example an approximate formula for predicting the maximum deflection y_{max} of a component in case of impulse sensitive structures is as follows [30]:

$$y_{max}(i) = \frac{1}{2}\left(\frac{(iA)^2}{(K_{LM}\ M)\ S_y} + d_y\right) \qquad (5)$$

In Eq. (5) A is the loaded area of the element, i is the impulse density of the demand, M is the total mass of the element, S_y and d_y are the yield resistance and displacement respectively of the element, and K_{LM} is the load-mass transformation factor (see following sections). The component must be assured to maintain y_{max} lower than the threshold value y_{LS} of the considered limit state. This can be simply done by comparing y_{LS} against the value of $y_{max}(\lambda i)$, where λ has been derived for the desired APE and the appropriate dispersions of demand and capacity. Note that a lognormal PDF is not necessarily preserved in the transformation of variables from structural response to intensity, thus Eq. (3) only becomes a rough but still useful approximation.

5 Hazard analysis of the case-study

To showcase the proposed approach, we shall consider a case-study of a blast-resistant door subject to accidental explosions of ammunitions. The steel built-up blast resistant door under consideration is located in the exterior side of a building belonging to a military facility. Along the side of the building there is a street transited by military vehicles carrying boxes of 60 mm mortar rounds in various quantities. Each metal ammunition box contains four High Explosive (HE) 60 mm mortar rounds, each containing 160 g (0.34 lb) of TNT [30]. The vehicles (jeep or van) generally carry about twelve ammunition boxes leading to a median explosive weight of 7.7 kg of TNT. At 25% and 75% of the cases, no more than ten and fifteen ammunition boxes are carried, respectively. Consequently a lognormal distribution with the coefficient of variation of 0.31 fits well with the total amount of explosive on an arbitrary military vehicle. Furthermore, the properties of the lognormal probability density function allow us to take into account rare cases where the vehicle is loaded over the “maximum considered” number of ammunition boxes.

As there are multiple identical blast doors along the length of the building, detonation is assumed to occur right opposite one of them, with the vehicle occupying any spot along the road cross-section with the same probability. With reference to Fig. 4, R_1 is the distance between the door and the edge of the road, R_2 is R_1 plus the sidewalk length, and finally R_3 is the distance from the detonation point to the sidewalk. R_2 is equal to 2m, while the stochastic variable R_3 is characterized by a uniform (non-informative) PDF between 0 and 7m. The stand-off distance is the sum of R_2 and R_3.

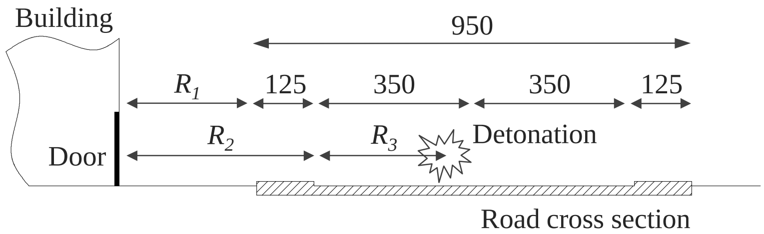

Fig. 4: Description of the blast scenario and of the considered variables; distances in [cm]

The lognormal PDF of the impulse density, shown in Fig. 5, is obtained by extracting 10^5 samples of both the explosive charge and the stand-off distance from their respective PDFs. The equivalent triangular pulse is computed as shown in Fig. 1a. All the terms in Fig. 1a are computed by the procedure proposed in the UFC 3-340-02 [2] manual. The resulting median value and dispersion of the impulse density demand are equal to 0.614 kPa sec and 0.601, respectively.

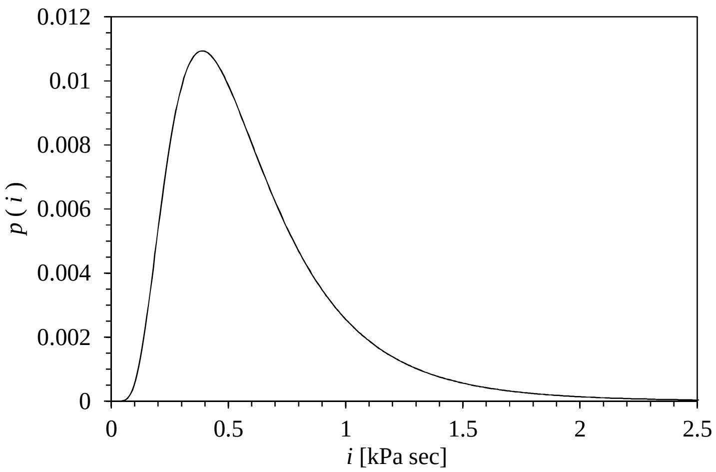

Fig. 5: Lognormal probability density function of the impulse density

6 Limit state definition for fragility analysis of the case-study

UFC 3-340-02 [2] provides the state of practice for designing structural elements against accidental explosions. A specific section of the UFC 3-340-02 [2] manual is focused on special considerations about blast resistant doors, where basic procedures and performance requirements are defined. More detailed design procedures for such elements are included in the Unified Facilities Guide Specifications (UFGS) 08-39-54 [39]. Blast resistant doors are conceived to contain an explosion and therefore prevent the propagation of pressure, fireball leakage and fragments inside the protected area [40 - 43].

There are different typologies of blast doors, classified on the basis of their structure (e.g. single leaf or double leaf) and on the basis of the opening mode (e.g. vertical lift and horizontal sliding). There are also several kinds of standard performance requirements for categorizing the blast doors according to their function. Performance requirements include:

- protection of personnel and equipment from external blast pressures resulting from an accidental explosion;
- prevention of accidental explosion propagation into an explosive storage area;
- maintain complete serviceability for doors designed as part of a containment cells commonly used in the repeated testing of explosives;
- maintain integrity for doors designed as part of containment structures commonly used to protect nearby personnel and structures in the event of an accidental explosion.

For our case-study a L_x = 2500 mm high and L_y = 1400 mm wide built-up steel door with a single leaf is considered. The door is made by welding steel plates to a steel beam grid. The grid is made up of UPN 80 beams on the boundaries that support four L 80x60/7 spandrel beams. On top of them, the exterior plate is 5 mm thick and the interior plate is 1 mm thick (see Fig. 6).

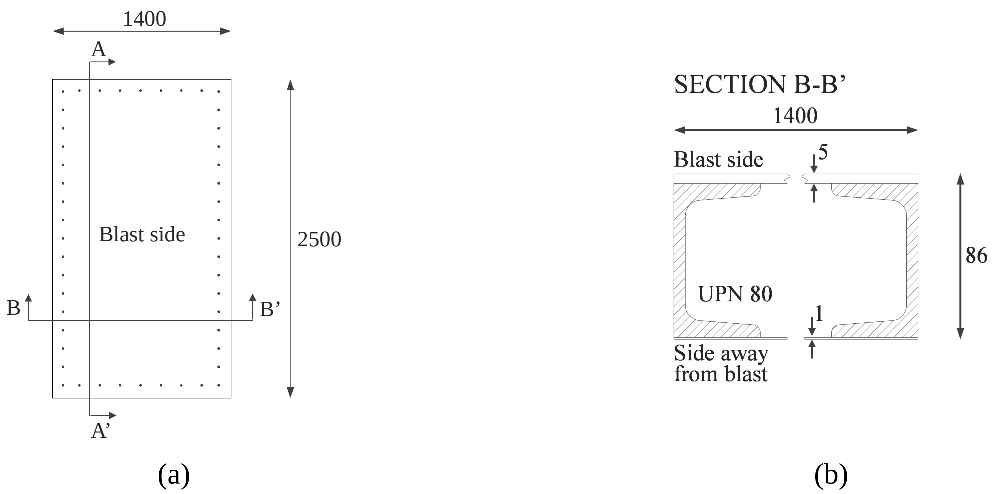

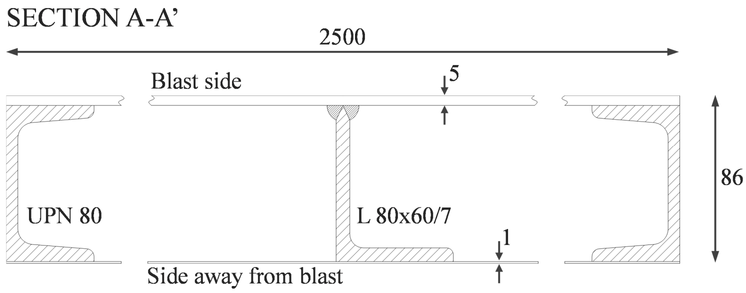

(c)

Fig. 6: Details of the case-study blast resistant door. Frontal view (a); section along the width (b); section along the height (c). Dimensions in [mm].

Adopting a performance-based philosophy four limit states are considered related to Serviceability, Operability, Life Safety and Critical Failure of the blast resistant door (Table 1). For this purpose one or more response parameters and appropriate threshold values of these parameters need to be defined. The selected response parameters are: the support rotation (θ) and the ductility ratio (m):

$$\theta = \arctan\left(\frac{2y_{max}}{L_y}\right) \qquad \text{(a)}$$

$$m = \frac{y_{max}}{d_y} \qquad \text{(b)} \qquad (6)$$

Where y_{max} is the maximum displacement of the component, d_y is the yield displacement (measured at the same position as the maximum), and L=L_y is the span of the component. In this case L_y is considered because, being shorter than L_x, it leads to a larger support rotation; more details are provided in the following sections.

A general consensus concerning the threshold values for the different limit states has not been reached in the scientific community. The adopted values have been chosen by means of a critical examination of both the literature and the physics of the problem, also with the support of appropriate numerical analyses described below. Note that different threshold values of a response parameter are expected for different typologies of the blast resisting doors. In order to give an idea of the uncertainty affecting the threshold values, a Qualitative Confidence Index (QCI) [44] is provided in the table, ranging from “high” (low level of uncertainty) to “low” (high amount of uncertainty).

The first limit state is Serviceability, the blast door should be fully operable after the event without need for repair. Damage to both the door structure and door accessories (like the panic opening system) is not allowed. The ductility ratio m is the response parameter chosen for this LS, with a threshold value (indicating violation) equal to 1.0. For Operability the door should be able to be opened. Damage to the door structure is allowed, but damage to the door accessories is not. Thus, the door should remain operable after the event, even if permanent deformations are present. This is important for avoiding failure and/or blockage of the panic opening system of the door in a way that both the evacuation of the building and the police/firemen operations can be easily conducted. In the case of Operability the support rotation is selected as the response parameter with a threshold value of 2 degrees [2, 42]. For Life Safety the inoperability of the door after the event is acceptable but the structure must not fail; significant permanent deflections of the door are still allowed; to satisfy the Life Safety criteria the support rotation is limited to a threshold value of 10 degrees. This value is chosen on the basis of the results obtained by a static pushover analysis of the case-study built-up door (see next sections). The last limit state is the Critical Failure and it occurs when the structural response of the door is causing the projection of the door itself or parts of it into the protected space.

Finally, as qualitatively assessed by the QCI, the dispersion on the thresholds defining the limit states can be taken into account by considering the threshold values as stochastic variables. By using Eq. (3) to estimate the safety factor, the dispersion of each limit state can be taken into account as shown in Eq. (7) where β_{LS} is the additional epistemic uncertainty dispersion of the limit state threshold.

$$\beta_T = \sqrt{\beta_C^2 + \beta_D^2 + \beta_{LS}^2} \tag{7}$$

Further investigations should be undertaken in order to assign a probability density function to the threshold values of the limit states in case of steel built-up blast resistant doors. Threshold values of the limit states are assumed here as deterministic parameters.

Limit State	**Serviceability**	**Operability**	**Life Safety**	**Critical Failure**
Damage level	The door has no permanent deflections	The door is operable, but it has permanent deflections	The door has not failed, but it has significant permanent deflections	The door has failed
Response parameter	Ductility ratio (m)	Support rotation (θ)	Support rotation (θ)	Support rotation (θ)
Threshold values	<1	<2°	<10°	>10°
QCI	High	Medium	Low	Low

Table 1: Considered limit states and threshold values

7 The Simplified Stochastic Model (SSM)

As early mentioned, a Simplified Stochastic Model (SSM) has been used to evaluate the fragility of the blast door. The SSM is an equivalent Single Degree of Freedom (SDOF) model of the steel built-up door, taking into account both the aleatory and epistemic uncertainties.

The equivalent SDOF system is obtained by evaluating appropriate transformation factors for the system's mass, damping, load and resistance. Furthermore, inherent within a SDOF analysis is the assumption that the system behaves only in a single deflection shape. In general, as the system begins to deflect under the blast load, it eventually yields and forms plastic hinges at various locations depending on the applied boundary conditions. Thus in reality, the system's mode shape changes with the progression of plastic hinges. Therefore, the transformation factors are adjusted to take into account the change of the mode shape. For a simply supported one way panel under uniform loading, it is assumed that a single plastic hinge is formed at the center of the element. The resistance-deflection relationship for such a panel is assumed to have an elastic-perfectly plastic shape. Thus, at a certain yield deflection, the component will continuously deform at near-constant resistance until an ultimate deflection limit is reached; at that point the component will fail. This resistance-deflection relationship (resistance function) serves as constitutive relation for the non-linear stiffness in the equation of motion.

The displacement field of the component can be expressed as $u(x,t)=\psi(x)y(t)$, where $\psi(x)$ is the assumed deformed shape of the component under the blast load and $y(t)$ is the displacement of the component at the location of maximum deflection at time t. Furthermore, displacement of the component is obtained by the SDOF equation:

$$K_{LM}M\ddot{y}(t) + C\dot{y}(t) + S\big(y(t)\big) = F(t) \quad (8)$$

where M is the total mass of the component, $S(y(t))$ is the resistance as a function of the displacement expressed in unit force, $F(t)$ is the blast pressure multiplied by the loaded area A expressed in force units, C is the damping (the percentage of the critical damping is assumed to be 1% in the analyses), K_{LM} is the load-mass transformation factor, that is equal to the ratio of K_M and K_L (the mass transformation factor and the load transformation factor respectively). The last two are evaluated by equating the energy of the two systems (in terms of work energy and kinetic energy respectively). The load-mass transformation factor K_{LM} is different at each deformation stage of the component response; for a bilinear resistance function two values of K_{LM} need to be defined: the first for the elastic and the second for the plastic range of the response [2, 45].

The built-up blast door considered is a two-dimensional orthotropic structure and it is made equivalent to a SDOF model with a bilinear resistance function. For obtaining such a resistance function, the yield point (P_y) needs to be defined, characterized by the yield blast pressure (r_y) and the corresponding yield displacement (d_y) of the door. In order to define the r_y and the d_y both aleatory and epistemic uncertainties are introduced.

In Eq. (6) the formulas for computing r_y and d_y are shown.

$$
\begin{aligned}
r_y &= \left(\frac{12}{L_x\,L_y}\right)\left(M_{px} + X_A\,M_{py}\right) && \text{(a)} \\
K_e &= X_B\,\frac{E\left(\frac{J_y}{L_x}\right)}{L_x\,{L_y}^3} && \text{(b)} \\
d_y &= \frac{r_y}{K_e} && \text{(c)}
\end{aligned}
\qquad (9)
$$

where, K_e is the stiffness of the SDOF, L_x and L_y are the longer and shorter dimensions of the door respectively, and E is the Young's modulus of steel. The coefficients X_A and X_B are taken equal to 1.374 and 198.6 respectively, and they are valid for orthotropic plates with L_y/L_x equal to 1.78 [2, 45, 46]. J_x and J_y are the moments of inertia, while M_{px} and M_{py} are the flexural plastic moments of the two orthogonal cross sections of the built-up door.

L_x, L_y, and E are assumed to be deterministic parameters, i.e., well known for a steel door; instead both J_y and J_x, and consequently M_{px} and M_{py} are considered as stochastic parameters in order to take into account the epistemic uncertainties. Moreover, the aleatory uncertainty affecting the yield stress of steel is considered.

With reference to Fig. 6 the door moments of inertia are computed by Eq. (10)

$$
\begin{aligned}
J_{x0} &= 2\,J_{UPN} + \left(L_y\,{t_1}^3\right)/12 + \left(L_y\,{t_2}^3\right)/12 && \text{(a)} \\
J_{y0} &= N_L\,J_L + 2\,J_{UPN} + \left[\left(L_x\,t_1\right)\left(\left(H_L + 0.5\,t_1\right) - d_G\right)^2\right] + \left[\left(L_y\,t_2\right)\left(0.5\,t_2 + d_G\right)^2\right] \\
&\quad + \left(L_y\,{t_1}^3\right)/12 + \left(L_y\,{t_2}^3\right)/12 && \text{(b)}
\end{aligned}
\qquad (10)
$$

where, N_L is the number of spandrels orthogonal to L_x, J_L and J_{UPN} are the moments of inertia of the spandrels and of the external frame respectively, t_1 and t_2 are the thicknesses of the plates on the blast side plate and the opposite side respectively, and d_G is the center of mass of the composite section. For computing J_{x0} the additional moment of inertia due to the plates is not considered because there are no spandrels connecting the plates along the L_x direction.

Noting that in the following the subscript "i" is adopted in order to indicate the single sample of the Monte Carlo simulation and the stochastic coefficient α is introduced to take into account the uncertainty of the moments of inertia. The sample values J_{xi} and J_{yi} are evaluated as shown in Eq. (11).

$$\begin{aligned} J_{xi} &= \alpha_i J_{x0} \quad \text{(a)} \\ J_{yi} &= \alpha_i J_{y0} \quad \text{(b)} \end{aligned} \qquad (11)$$

M_{pxi} and M_{pyi} are computed by Eq. (12) considering also Eq. (13).

$$\begin{aligned} M_{pxi} &= \sigma_{ydi}\, \varphi_i\, \alpha_i \frac{J_{xi}}{b_x} \quad \text{(a)} \\ M_{pyi} &= \sigma_{ydi}\, \varphi_i\, \alpha_i \frac{J_{yi}}{b_y} \quad \text{(b)} \end{aligned} \qquad (12)$$

$$\begin{aligned} \sigma_{ydi} &= \sigma_{yi}\, DIF_i \quad \text{(a)} \\ DIF_i &= 1 + DIF_{0i} \quad \text{(b)} \\ \varphi_i &= 1 + \varphi_{0i} \quad \text{(c)} \end{aligned} \qquad (13)$$

In the above equations b_x and b_y are the longest distances between the center of mass and each of the two external sides of the cross sections, while σ_{ydi} and σ_{yi} are the sample values of the dynamic and static yield stress of steel, respectively, assumed to be random. The sample value DIF_i of the Dynamic Increase Factor, is obtained as one plus the decimal part DIF_{0i}, the latter assumed to be random to consider epistemic uncertainty. Finally ϕ_i is the sample value of the plastic coefficient obtained as one plus the decimal part ϕ_{0i}; ϕ_{0i} is assumed as a stochastic variable affected by uncertainty.

The considered stochastic variables are summarized in Table 2 together with their distribution characteristics. The mean value of α is set equal to unity; the mean value of σ_y is estimated by assuming a strength factor equal to 1.1 [45], leading to a mean value of σ_y equal to 302.5 MPa for a steel having tensile strength equal to 450 MPa; the mean value of ϕ is estimated by fitting the resistance of the SSM with the static pushover curve computed by the FE model as described in what follows; finally the mean value of the *DIF* is provided in the Methodology Manual for the SDOF Blast Effects Design Spreadsheets [45] for an equivalent grade of steel. With regard to the dispersion of these coefficients, the coefficient of variation of σ_y is taken from the study of Enright and Frangopol [47]; while the coefficient of variation of both α and ϕ are estimated by means of the dispersion of P_y with respect to the static pushover curve obtained by the FE model. The coefficient of variation of the *DIF* is estimated by the values of the *DIF* provided by the Methodology Manual for the SDOF Blast Effects Design Spreadsheets [45] for several strain rate velocities.

Parameter	Median value	*COV*	Distribution
σ_y	302.5 MPa	0.12	lognormal
α	1	0.1	lognormal
ϕ_0	0.3	0.1	lognormal
DIF_0	0.19	0.2	lognormal

Table 2: Probabilistic distributions of the stochastic variables

By substituting the sample values obtained in Eq. (11), (12) and (13) into the Eq. (9), the sample P_{yi} of the yield point P_y of the resistance function is computed. The resulting median value of r_u and d_y are 306 kPa and 6.8 mm respectively, while their coefficient of variation are 0.16 and 0.125 respectively.

8 Validation of the SSM by the Finite Element model

In order to validate the SSM a detailed Finite Element Model (FE model) is developed, using the commercial FE solver LS-Dyna® [48] and employing shell elements for the constituent parts of the blast door. The support frame of the door is also explicitly modeled in order to accurately take into account the unilateral boundary conditions by making use of contact elements. Additional contact elements are provided for the door opening hinges and door locking system for allowing the rebound response. In total the model consists of 84794 shell elements and 85062 nodes. The shell elements are of Belytschko-Tsay type [48] and the contact algorithm is the automatic surface to surface [48].

With regard to steel, a piecewise linear plasticity model [48] is adopted, see Fig. 7. The engineering stress-strain curve is taken from the study of Kalochairetis et al. [49] by a quasi-static experimental test considering the length and the initial cross sectional area of the specimen; instead the true stress-strain curve is obtained analytically by assuming logarithmic strains [48]. Furthermore, a fracture criterion is implemented without taking into account the effect of the stress triaxiality; the fracture occurs when the effective plastic strain reaches the value 0.2473 corresponding to the maximum resisting stress before softening. The strain rate effect is taken into account by a *DIF* computed by the Cowper and Symonds model shows in Eq. 14 [48], where ξ is equal to 500 [1/s] and γ is equal to 6 [45].

$$DIF = 1 + \left(\frac{\dot{\varepsilon}}{\xi}\right)^{\frac{1}{\gamma}} \quad (14)$$

It is crucial to highlight that the steel yield stress shown in Fig. 7 does not match the mean value of the steel yield stress of Table 2. In order to validate the SSM by the FE model, the input parameters are assumed to have the mean values and the steel stress-strain relationship shown in Fig. 7. Furthermore a *DIF* equal to 1 and 1.19 for the case of the static and dynamic response respectively has been assumed for the SSM.

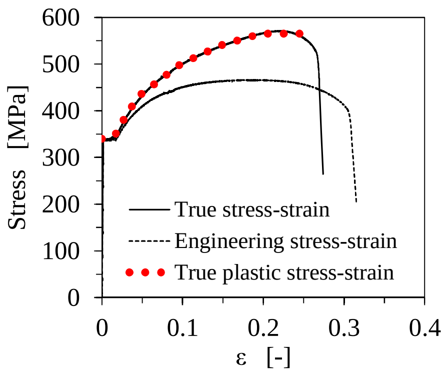

Fig. 7: Stress strain relationship [49]

In Fig. 8a the FE model and details of the built-up door are shown. A magnified view of the FE model is presented in Fig. 8a. The characteristic dimension of the single rectangular finite element is 15 mm and it is quite constant for the entire mesh. As needed, a sensitivity analysis has been conducted regarding the mesh refinement, whose results are not reported here for the sake of brevity.

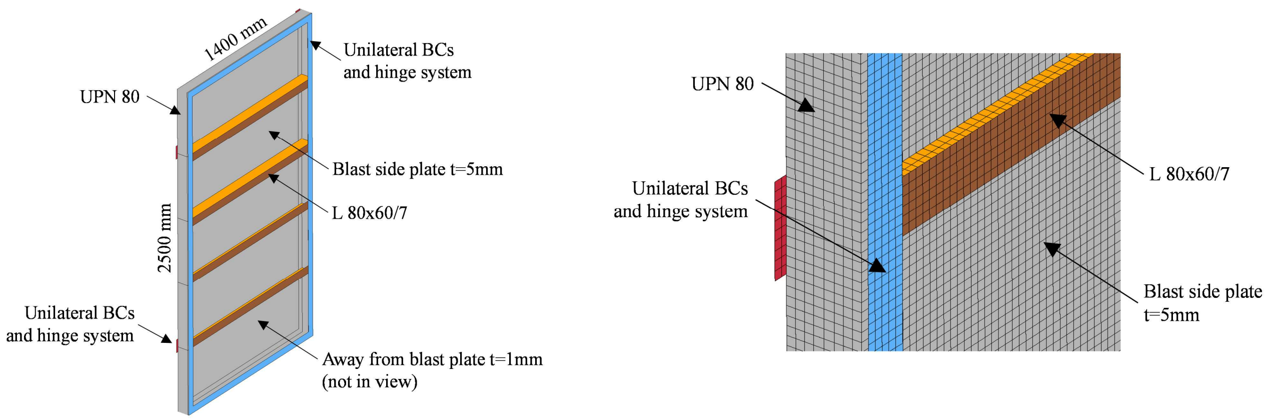

(a) (b)

Fig. 8: Details of the FE model used in the analyses

8.1 Deterministic static resistance function

In order to obtain the static resistance function of the built-up blast door a static pushover analysis is carried out by applying a uniform load to the blast side plate. The uniform pressure is applied quasi-statically by a ramp load function until the collapse of the door is reached. In Fig. 9 the static resistance functions computed by the SSM (by assuming the mean values of the input parameters) and the FE model are shown. In Fig. 9a the static resistance function is plotted as a function of the mid-span displacement *y*, while in Fig. 9a it is plotted as a function of the support rotation θ defined in Eq. 6. Especially for the range of support rotation from 0 to 2 degrees there is a good agreement between the two predictions, while introducing a positive stiffness post-yield stress-strain model would easily extend this to rotations of 6 degrees or more. However, only appropriate experimental tests could fully confirm the results.

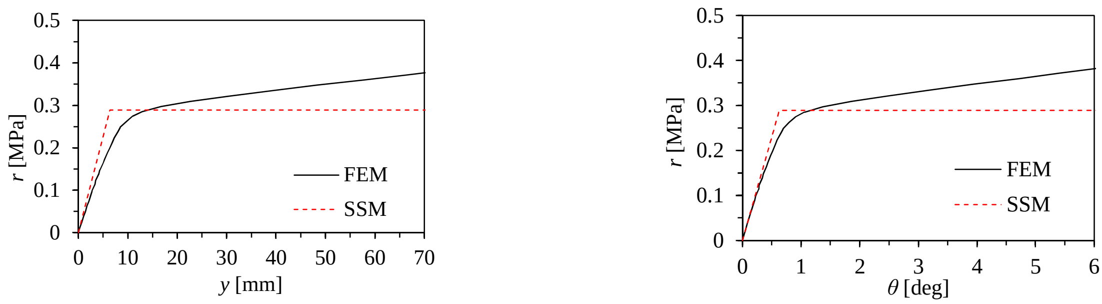

(a) (b)

Fig. 9: Static resistance function of the case-study door (the adopted steel is the one having the stress-strain relationship shown in Fig. 7).

8.2 Deterministic dynamic structural response

The FE model and the SSM are then compared in terms of dynamic structural response. The built-up door is subjected to four detonations and the structural response is computed by both the SSM and the FE model. All the detonations occur at 500 mm from the ground and at 6 m away from the door. The explosive charges of the four detonations are assumed to consist of 10, 15, 20, 25 kg of TNT. The blast pressure is assumed as uniformly distributed in the SSM, but it is properly evaluated as non-uniformly distributed in the FE model by the LS-Dyna® function named load blast [48]. Only the positive phase of the shock wave is taken into account by the equivalent triangular pulse, alternatively an exponential decay law can be adopted [35].

Concerning the parameters characterizing the SSM, the values adopted for comparison purposes with the FE model are: σ_y=340 MPa, ϕ=1.3, α=1, and *DIF*=1.19; thus it is important to recall that, as mentioned above, for the successive computations of the fragility curves and of the safety factor, the mean value of σ_y is assumed to be 302.5 MPa. In Fig. 10 the comparison between the time histories of the support rotation θ obtained with the FE model and the SSM are reported for all the four detonations.

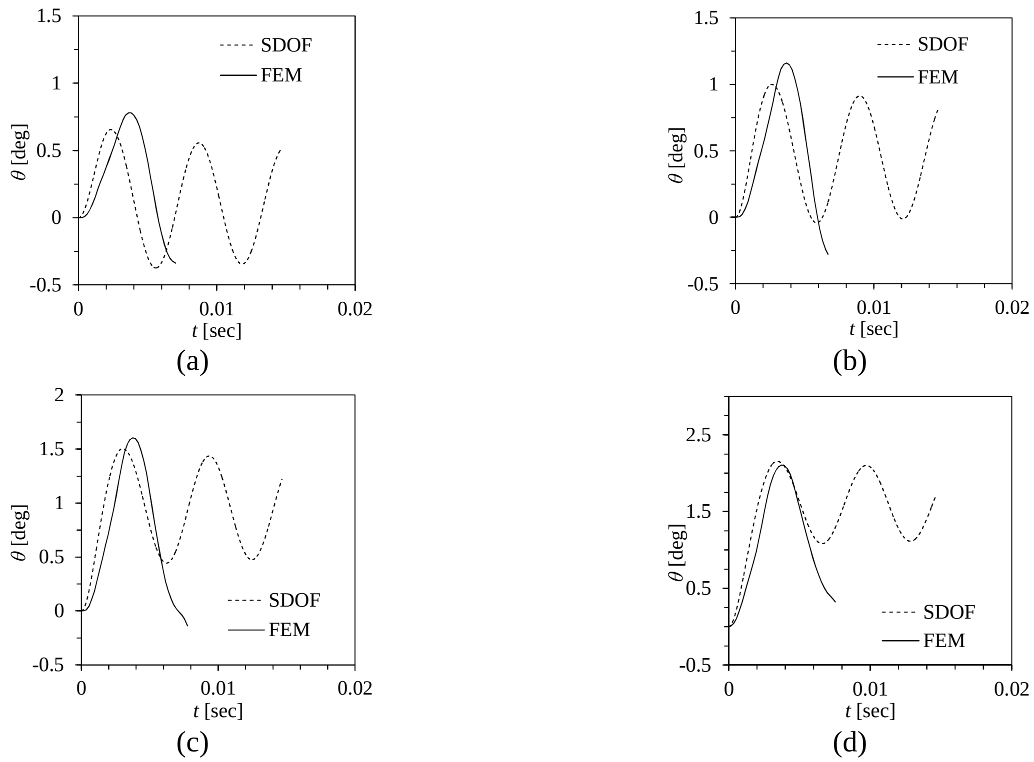

Fig. 10: Comparison between the time histories of the support rotation θ obtained with the FE model and the SSM (SDOF in legend). 10 kg of TNT (a); 15 kg of TNT (b); 20 kg of TNT (c); 25 kg of TNT (d).

In Fig. 11, where the boundary conditions and plate opposite to the blast side are removed from the view for allowing the checking of the spandrels, the plastic strains on the door obtained by the FE model are plotted. Plastic strains are represented in black color while in grey is the elastic steel (in the black zones the dynamic yield stress of the steel was reached).

With reference to Fig. 10 it can be appreciated that generally there is a good agreement between the predictions of the support rotations obtained by the SSM and the FE model. However the SSM seems to be slightly conservative with respect to the FE model. Furthermore due to the non-linear boundary conditions implemented in the FE model, the rebound response and the time of the max support rotation are somewhat different, but this is not relevant for the purpose of the SSM that is to estimate only the maximum support rotation of the built-up door.

It is noteworthy that the SDOF can well predict the deflection but no local damage. However, the SDOF is able to predict the global behavior of the door and its failure due to excessive mid-span displacement or support rotation, something that is sufficient for the purposes of this paper, with enormous reduction of the computational effort with respect to the FE analysis.

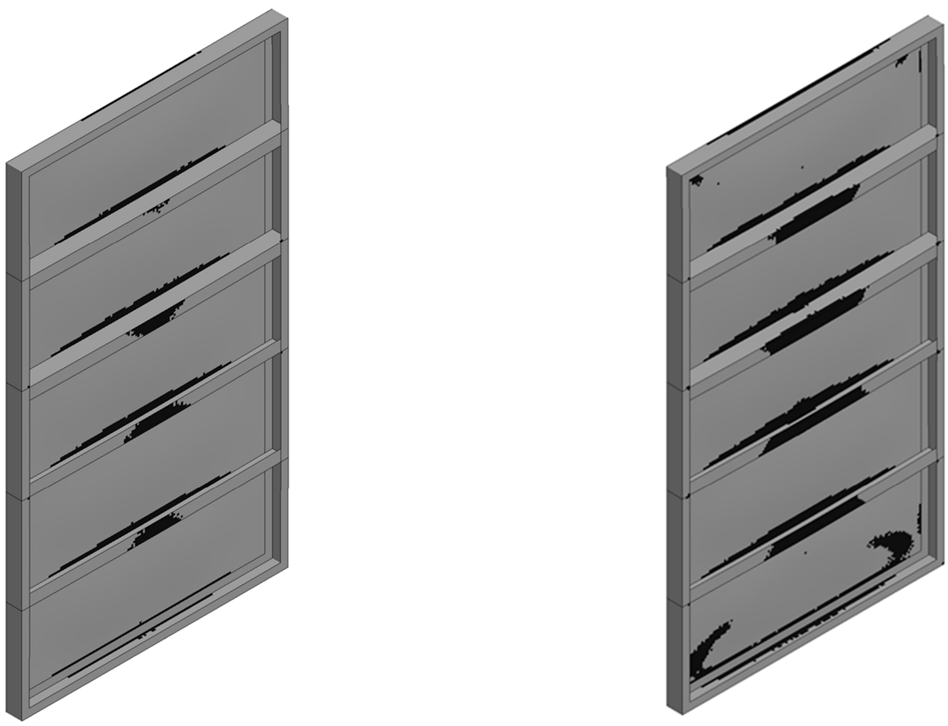

(a) (b)

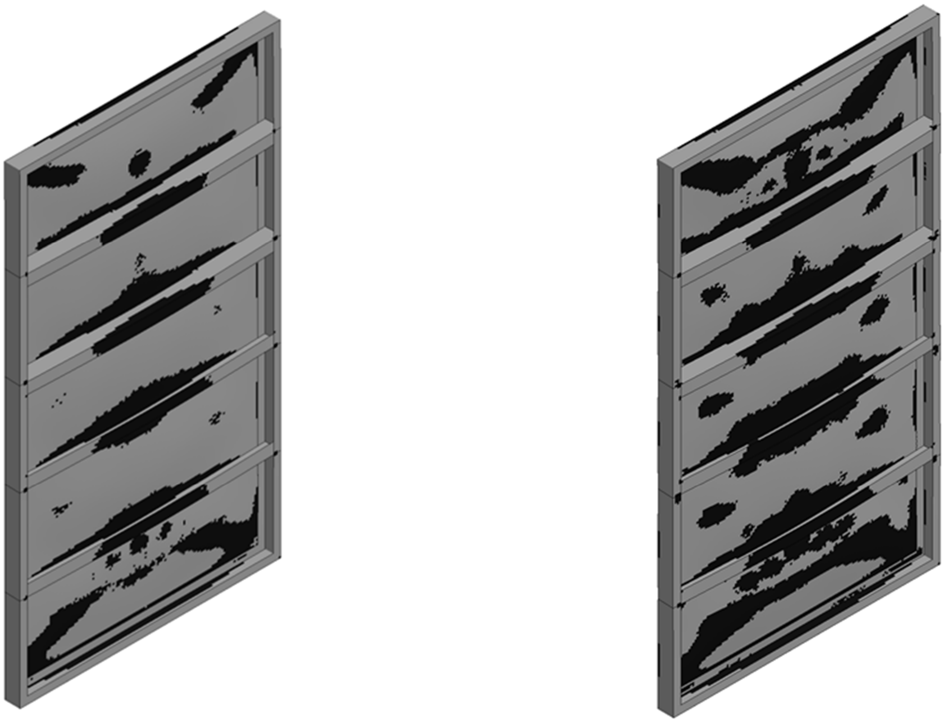

(c) (d)

Fig. 11: Plastic strains on the door obtained by the FE model. 10 kg of TNT (a); 15 kg of TNT (b); 20 kg of TNT (c); 25 kg of TNT (d).

On the basis of the plastic strain results shown in Fig. 11, it can be stated that the non-uniform distribution of the blast load does not lead to a particularly non-uniform structural response of the built-up door: the plastic strains on the spandrels are quite uniform. Furthermore, it can be argued that the door develops a flexural resistant mechanism since only limited plasticity is developed at the connection of the spandrels with the external frame. In the case of 25 kg of TNT, Fig. 11(d), the blast side plate shows spread of plasticity but it maintains the ability to transfer the load on the spandrels; note that the previously mentioned fracture criterion is implemented in the FE model and an eventual fracture of the blast side plate would be detected.

9 Computing the fragility curves

In this section the fragility curves for the built-up blast door are developed for each limit state previously defined. The fragility curve is computed point by point using a Monte Carlo- based algorithm [24] and the resulting points are fit by a lognormal CDF in order to obtain a smooth curve to use in computing the probability of exceeding the limit state and the corresponding safety factor. The flowchart representing the steps in computing the fragility curves is shown in Fig. 12. Looking at the flowchart, N is the number of the points in which the fragility curve is numerically evaluated, j is the loop counter identifying the Monte Carlo simulation which is performed to evaluate the single point FC(j) of the fragility curve, corresponding to the *j-th* value IM_j of the intensity measure (impulse density). For j=1 a Monte Carlo simulation is carried out and the conditional probability of exceedance is estimated. The next step is to compute the successive point of the fragility curve, then for the new value of the *IM* a new Monte Carlo simulation is performed and the conditional probability of exceedance is estimated. This cycle is repeated until j=N.

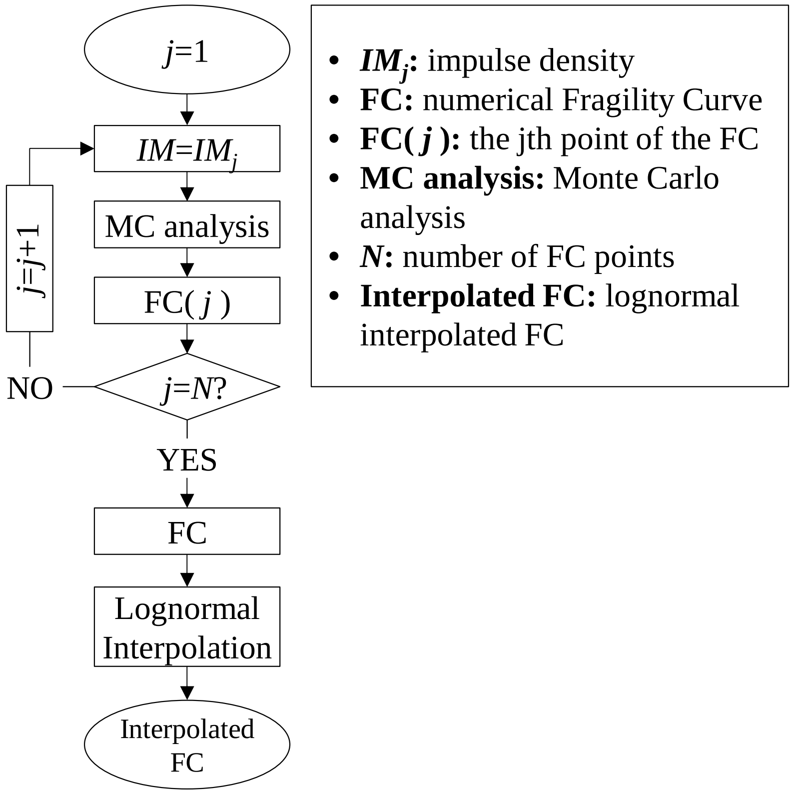

Fig. 12: Flowchart of the procedure for the evaluation of the fragility curves. FC= fragility curve.

The first fragility curve obtained by the algorithm shown in the flowchart of Fig. 12 is called “numerical fragility curve”. The final step consists of fitting the points of the numerical fragility curve in order to obtain the analytic lognormal fragility curve defined by the mean value and the standard deviation of the corresponding normal. In Fig. 13 the fragilities curves obtained for the Serviceability, Operability, and Life Safety limit states are shown. Their median values (μ_{ln}) and coefficient of variations (β_{ln}) are shown in Table 3.

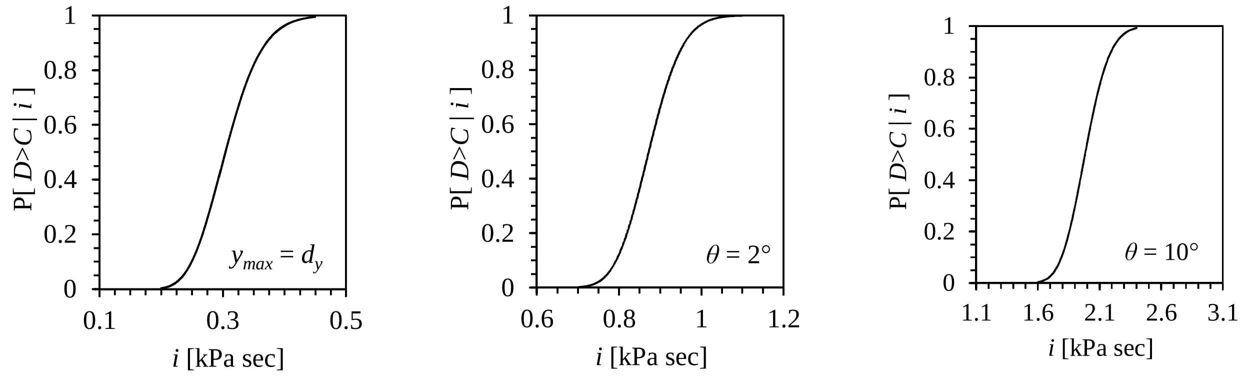

(a) (b) (c)

Fig. 13: Fragility curves obtained by the SSM. Serviceability (a), Operability (b), and Life Safety (c)

Limit State		Serviceability	Operability	Life Safety	Critical Failure
Response Parameter		$y < d_y$	$\theta < 2°$	$\theta < 10°$	$\theta > 10°$
FC	μ_{ln} [kPa sec]	0.3080	0.8700	1.9800	1.9800
	β_{ln}	0.1518	0.0748	0.0785	0.0785

Table 3: Characterization of the fragility curves for the examinated limit states.

The number of samples (N_j) used in the Monte Carlo simulation to compute the single point FC(j) of the numerical fragility curve is not constant; N_j is chosen for each j in order to maintain the coefficient of variation (COV_j) of the estimated value (representative of the error due to sampling) under a maximum acceptable threshold. The COV_j is quantified as:

$$COV_{j_{\mathrm{P}[D>C|\, i_j]}} = \sqrt{\frac{1 - \mathrm{P}\left[D > C|\, i_j\right]}{\mathrm{P}\left[D > C|\, i_j\right] N_j}} \quad (15)$$

With regard to the fragility curve associated with the Operability limit state, the variation of both the number of samples and coefficient of variation with the conditional exceedance probability $\mathrm{P}[D > C|\, i]$ is shown in Fig. 14. The number of samples decreases exponentially from the lowest to the highest probability of the numerical fragility curve. Regardless of the *COV*, though, a practical maximum and minimum number of samples of 10^5 and 10^3 respectively, is adopted. As shown in Fig. 14 the maximum coefficient of variation is less than 0.1 for a conditional exceeding probability of 0.001 and it decreases quickly; for example it is less than 0.02 for a $\mathrm{P}[D > C|\, i]$ of 0.1.

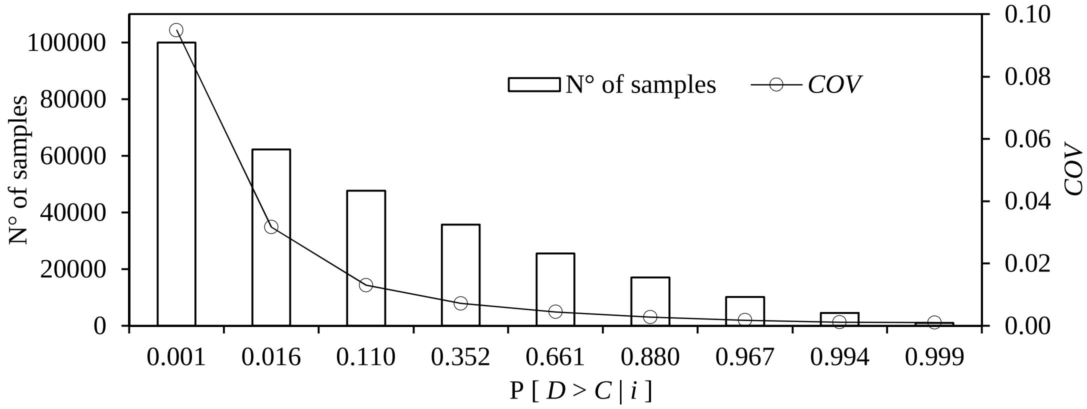

Fig. 14: Variation of both N_j and *COV* with P[D>C| i] for the Operability limit state

507 ## 10 Performance assessment

Following the conditional approach, Eq. (1) can be evaluated numerically by making use of the fragility curve P[D>C|i] and of the probability density function of the impulse density *f(i)* shown in Fig. 5:

$$\mathrm{P}[D > C] = \int_{-\infty}^{+\infty} \mathrm{P}[\, D > C \mid i \,]\, f(i)\ \partial i \cong \sum_{j=0}^{N} \mathrm{P}\big[D > C \mid i\,\big]_j\ f(i)_j\ \Delta i_j \quad (16)$$

Table 4 provides the probabilities of exceedance computed by both the conditional and unconditional approaches.

$\widehat{W}$ = 7.7 kg *COV*=0.3 lognormal distribution
R_2 = 2 m $0 \le R_3 \le 7$ uniform distribution

Limit State	**Conditional Approach (CA)**	**Unconditional Approach (UA)**	**Δ=CA-UA**	**Closed-form Solution (Eq. 2)**
Serviceability	0.8303	0.6343	0.1960	0.8553
Operability	0.1830	0.2065	-0.0230	0.2490
Life Safety	0.0195	0.0078	0.0117	0.0179

Table 4: Probabilities of exceedance obtained with the conditional and unconditional approaches versus the simplified closed-form solution.

For the Operability and the Life Safety limit states both the conditional and the unconditional approach provide quite the same probability of exceedance, the slight difference between the two approaches is probably due to the differences in the coefficient of variations of the computed probabilities of exceedance (Fig. 14). On the other hand, for the Serviceability limit state the difference between the two estimations is greater than in the previous cases and the probability of exceedance computed by the conditional approach is higher. This is because the hypothesis of impulsive loading is not respected as can be argued from Fig. 15 and detailed below. For all practical purposes, as long as the structure is impulsively loaded, the two methods can be considered to be almost the same.

By adopting the mean values of the above mentioned stochastic parameters (see Table 2 and Eq. 13), the pressure-impulse curves corresponding to each limit states (average pressure-impulse curves) are obtained by the SSM and shown in Fig. 15. Therein the *IM* samples used in the evaluation of the probabilities of exceedance are plotted, showing that the *IM* samples fall in the impulsive region for the Operability and Life Safety limit states, while they fall close at least to the dynamic region for the Serviceability limit state.

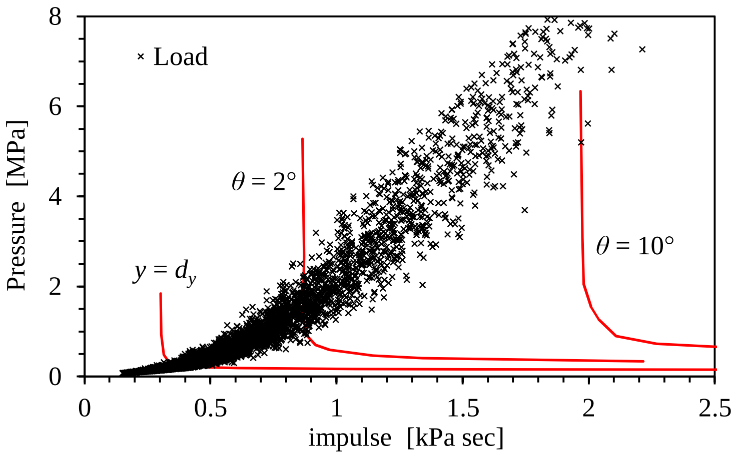

Fig. 15: Load samples and their relative position with respect to the average pressure-impulse curves related to the considered limit states

Finally, in Fig. 16 the safety factor obtained for the case-study blast resistant door via Eq. (3) is plotted as function of the acceptable probability of exceedance (APE) for the Serviceability, Operability, and Life Safety limit states.

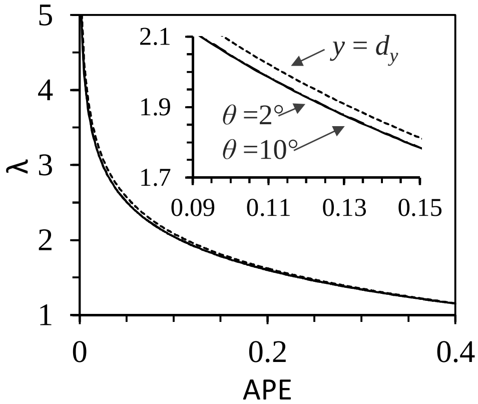

Fig. 16: Safety factor as function of the acceptable probability of exceedance. The θ=2° and θ=10° curves are practically coincident.

From Eq. 3a the dispersion measure β_T depends on the dispersion of both the capacity and the demand. In the case study, looking also at Table 3, the dispersion of the capacities obtained from the fragilities related to the Operability and Life Safety limit states are practically the same; this leads to a nearly identical safety factor as a function of the acceptable probability of exceedance for these two limit states, as shown in Fig. 16. Concerning the Serviceability limit state, the coefficient of variation of the capacity is greater than the ones of the Operability and Life Safety limit state (see Table 3), but it still remains quite small with respect to the dispersion of the demand (which is equal to 0.601 as said in section 5). In other words, the dispersion due to the structural model uncertainty is vastly inferior to the dispersion of the hazard (something that has also been observed for other hazards as well, e.g. earthquakes) and the latter obviously dominates.

For illustrative purposes, the dispersion on the threshold value of the Operability limit state is added in computing the total dispersion shown in Eq. (4) as shown in Eq. (7), thus the updated safety factor is compared with the one shown in Fig. 16 for an APE of 0.2. The probability density function of the limit state threshold value is assumed as lognormal with a dispersion of 0.4, therefore Eq. (7) provides a total dispersion equal to 0.68, and consequently the safety factor $\lambda(0.2)$ is equal to 1.77. Considering that the original $\lambda(0.2)$ is equal to 1.6, it is evident that adding the dispersion to the threshold value of the limit state increases the value of the safety factor. As long as this additional variability is inferior to the impulse hazard dispersion (0.4 versus 0.6), the square-root-sum-of-squares combination rule in Eq. (8) means that the hazard still dominates and the safety factor remains relatively similar. Otherwise, it should be expected to increase substantially.

Finally, a practical example is presented on using the proposed safety factor to perform a simple assessment of the steel blast resistant door. Let us consider the Operability limit state (θ=2°). The median resistance function is defined by the yield point values of r_u and d_y equal to 306 kPa and 6.8

mm respectively, while the median value of the impulse density is 0.614 kPa sec. Both the median values of the yield point and of the impulse density are computed by extracting samples as shown in the previous sections. By applying Eq. (5) without regard for variability, the maximum support rotation is 1.4°, thus the Operability limit state is thought to be satisfied. However, by applying Eq. (5) using the safety factor $\lambda(0.2)$ equal to 1.6 (see Fig. 16) the maximum support rotation becomes 3.1°, meaning that the Operability limit state is not satisfied due to the effect of uncertainties.

11 Conclusions

An investigation has been conducted on the use of simplifying approaches for probabilistically estimating the performance of structures subject to blast hazard. First, a conditional approach has been introduced using the impulse density as a sufficient intensity measure (*IM*) for decoupling the evaluation of blast hazard and the determination of structural response for impulse-governed case studies. This essentially reduces the, otherwise necessary, Monte Carlo simulation into the evaluation of the *IM* hazard distribution and the fragility of the structural system, and thus decreases the computational load by several orders of magnitude. Second, a safety factor approach, similar to existing load-and- resistance-factored design (LRFD) formats, has been suggested to offer even simple estimates of the probability of violating the limit state. Moreover, the relationship between the fragility (surface and curve) and the pressure-impulse diagram of a component has been clarified.

A steel built-up blast resistant door was employed as a tested to determine the probability of exceedance through the conditional, the unconditional, and the safety factor approach. As expected, as long as the component demand is governed by an impulsive load, the conditional method based on the impulse density can significantly reduce the computations needed to determine the system's performance. The proposed closed-form safety factor managed to offer a practical estimate of the probability of limit-state violation at the expense of some additional error. Moreover, such analytic solutions were shown to offer useful insight. For example, as known in other fields of engineering, when the dispersion of the demand is greater than the dispersion of the capacity, the overall estimates of probability mainly depend on the hazard rather than the model uncertainty. Thus, one can often forego the variability in the model without biasing the analysis. In summary, we hope that the groundwork has been established for using simplified probabilistic procedures for the Performance-Based Design (PBD) of structures subjected to blast.

12 Acknowledgements

The support of Prof. Franco Bontempi and Dr. Konstantinos Gkoumas of the Sapienza University of Rome are gratefully acknowledged. The authors would like to acknowledge the contribution of Dr. K. Kalochairetis (NTUA) for providing test data of the steel stress-strain relation. This work was partially supported by StroNGER s.r.l. from the fund “FILAS - POR FESR LAZIO 2007/2013 - Support for the research spin off” and the EU Research Executive Agency via the Marie Curie Continuing Integration Grant No. PCIG09-GA-2011-293855. Furthermore this manuscript has been published under the tenure of the International Research Fellow of the Japan Society for Promotion of Science grant number P-15786.

13 References

1 Netherton MD, Stewart MG. Blast load variability and accuracy of blast load prediction models. International Journal of Protective Structures 2010; 1(4): 543-570.

2 Unified Facilities Criteria (UFC). Structures to resist the effects of accidental explosions (UFC 3-340-02). United States Department of Defense; 2008.

3 Stewart MG. Risk-informed decision support for assessing the costs and benefits of counter-terrorism protective measures for infrastructure. International Journal of Critical Infrastructures Protection 2010; 3: 29-40.

4 Yu J, Tan KH. Experimental and numerical investigation on progressive collapse resistance of reinforced concrete beam column sub-assemblages. Engineering Structures 2013; 55: 90-106.

5 Olmati P, Gkoumas K, Brando F, Cao L. Consequence-based robustness assessment of a steel truss bridge. Steel and Composite Structures 2013; 14(4): 379-395.

6 Ballantyne GJ, Whittaker AS, Dargush GF, Aref AJ. Air-blast effects on structural shapes of finite width. Journal of Structural Engineering 2010; 136(2): 152-159.

7 Olmati P, Petrini F, Bontempi F. Numerical analyses for the structural assessment of steel buildings under explosions. Structural Engineering and Mechanics 2013; 45(6): 803-819.

8 Naito C, Hoemann J, Beacraft M and Bewick B. Performance and characterization of shear ties for use in insulated precast concrete sandwich wall panels. Journal of Structural Engineering 2012; 138(1): 1-11.

9 Stewart MG, Netherton MD. Security risks and probabilistic risk assessment of glazing subject to explosive blast loading. Reliability Engineering and System Safety 2008; 93: 627–638.

10 Netherton MD, Stewart MG. The effects of explosive blast load variability on safety hazard and damage risks for monolithic window glazing. International Journal of Impact Engineering 2009; 36: 1346-1354.

11 Wu C, Oehlers DJ, Rebentrost M, Leach J, Whittaker AS. Blast testing of ultra-high performance fibre and FRP-retrofitted concrete slabs. Engineering Structures 2009; 31: 2060-2069.

12 Chang DB, Young CS. Probabilistic estimates of vulnerability to explosive overpressures and impulses. Journal of Physical Security 2010; 4(2): 10-29.

13 Low HY, Hao H. Reliability analysis of reinforced concrete slabs under explosive loading. Structural Safety 2001; 23: 157-178.

14 Olmati P, Petrini F, Gkoumas K. Fragility analysis for the Performance-Based Design of cladding wall panels subjected to blast load. Engineering Structure 2014; 78: 112-120.

15 Kennedy RP, Ravindra MK. Seismic fragilities for nuclear power plant risk studies. Nuclear Engineering and Design 1984; 79: 47-68.

16 Reed JW, Kennedy RP. Methodology for developing seismic fragilities (report TR-103959). Jack R. Benjamin and Associates, Inc. and RPK Structural Mechanics Consulting, Electric Power Research Institute; 1994.

17 Spence SMJ, Gioffrè M. Large scale reliability-based design optimization of wind excited tall buildings. Probabilistic Engineering Mechanics 2012; 28: 206–215.

18 Shinozuka M, Feng MQ, Lee J, Naganuma T. Statistical analysis of fragility curves. Journal of Engineering Mechanics 2000; 126(12): 1224-1231.

19 Wen YK, Ellingwood BR. The role of fragility assessment in consequence-based engineering. Earthquake Spectra 2005; 21(3): 861-877.

20 Fyllingen Ø, Hopperstad OS, Langseth M. Stochastic simulations of square aluminium tubes subjected to axial loading. International Journal of Impact Engineering 2007; 34: 1619-1636.

21 Lange D, Devaney S, Usmani A. An Application of the PEER PBEE Framework to Structures in Fire. Engineering Structures 2014; 66: 100-115.

22 Sgambi L, Garavaglia E, Basso N, Bontempi F. Monte Carlo simulation for seismic analysis of a long span suspension bridge. Engineering Structures 2014; 78: 100–111.

23 Barbato M, Palmeri A, Petrini F. Special Issue on Performance-based engineering. Editorial foreword. Engineering Structures 2014; 78: 1-2. .

24 Olmati P, Trasborg P, Naito CJ, Bontempi F. Blast resistant design of precast reinforced concrete walls for strategic infrastructures under uncertainty. International Journal of Critical Infrastructures 2015; 11(3): 197-212.

25 Bazzurro P, Cornell CA, Shome N, Carballo JE. Three proposals for characterizing MDOF nonlinear seismic response. Journal of Structural Engineering 1998; 124(11): 1281-1289.
26 Fragiadakis M, Vamvatsikos D, Karlaftis MG, Lagaros ND, Papadrakakis M. Seismic assessment of structures and lifelines. Journal of Sound and Vibration 2015; 334: 29-56.
27 Luco, N., and C.A. Cornell. Structure-specific scalar intensity measures for near-source and ordinary earthquake ground motions. Earthquake Spectra 2007; 23(2): 357-392
28 Ciampoli M, Petrini F. Performance-Based Aeolian Risk assessment and reduction for tall buildings. Probabilistic Engineering Mechanics 2012; 28: 75-84.
29 Cornell CA, Jalayer F, Hamburger RO, Foutch DA. Probabilistic Basis for 2000 SAC Federal Emergency Management Agency Steel Moment Frame Guidelines. Journal of Structural Engineering 2002; 128(4): 526-533.
30 Krauthammer T. Modern protective structures. New York: CRC Press, Taylor & Francis Group, 2008.
31 Scherbatiuk K, Rattanawangcharoen N, Pope DJ, Fowler J. Generation of a pressure–impulse diagram for a temporary soil wall using an analytical rigid-body rotation model. International Journal of Impact Engineering 2008; 35: 530-539.
32 Krauthammer T, Astarlioglu S, Blasko J, Soh TB, Ng PH. Pressure-impulse diagrams for the behavior assessment of structural components. International Journal of Impact Engineering 2008; 35: 771-783.
33 Shi Y, Hao H, Hao ZX. Numerical derivation of pressure–impulse diagrams for prediction of RC column damage to blast loads. International Journal of Impact Engineering 2008; 35: 1213-1227.
34 Yim HC, Krauthammer T. Load–impulse characterization for steel connection. International Journal of Impact Engineering 2009; 36: 737-745.
35 Gantes CJ, Pnevmatikos NG. Elastic–plastic response spectra for exponential blast loading. International Journal of Impact Engineering 2004; 30: 323-343.
36 Ma GW, Shi HG, Shu DW. P–I diagram method for combined failure modes of rigid-plastic beams. International Journal of Impact Engineering 2007; 34: 1081-1094.
37 Fallah AS, Louca LA. Pressure–impulse diagrams for elastic-plastic-hardening and softening single-degree-of-freedom models subjected to blast loading. International Journal of Impact Engineering 2007; 34: 823-842.
38 Cornell CA. A probability-based structural code. Journal of the American Concrete Institute 1969: 66(11).

39 Unified Facilities Guide Specifications (UFGS). Blast Resistant Doors (UFGS 08-39-54). The United States Army Corps of Engineers (USACE); 2009.
40 Mayorga MA. The pathology of primary blast overpressure injury. Toxicology 1997; 121: 17-28.
41 Stuhmiller JH, Ho KH, Vander Vorst MJ, Dodd KT, Fitzpatrick T, Mayorga M. A model of blast overpressure injury to the lung. Journal of Biomechanics 1996; 29(2): 227–234.
42 Chen W, Hao H. Numerical study of a new multi-arch double-layered blast-resistance door panel. International Journal of Impact Engineering 2012; 43: 16-28.
43 Xingna L, Xinming Q, Huanjuan Z, Ping H. Simulation analysis on structure safety of refuge chamber door under explosion load. Procedia Engineering 2012; 45: 923-929.
44 Garavaglia E, Sgambi L. The use of a credibility index in the life-cycle assessment of structures. Structure and Infrastructure Engineering 2015; 11(5): 683-694.
45 Methodology Manual for the Single-Degree-of-Freedom Blast Effects Design Spreadsheets (TR-06-01 Rev 1). The United States Army Corps of Engineers (USACE); 2008.
46 Biggs JM. Introduction to structural dynamics. New York: McGraw-Hill; 1964.
47 Enright MP, DM Frangopol. Probabilistic analysis of resistance degradation of reinforced concrete bridge beams under corrosion. Engineering Structures 1998; 20(11): 960-971.
48 Hallquist J. LS-DYNA theory manual. Livermore (CA): Livermore Software Technology Corp.; 2012.
49 Kalochairetis KE, Gantes CJ, Lignos XA. Experimental and Numerical Investigation of Eccentrically Loaded Laced Built-Up Steel Columns. Journal of Constructional Steel Research 2014; 101: 66-81.